M-SPURT—Compressing the target characterization for a fast monostatic RCS simulation

Henna Perälä, Minna Väilä, and Juha Jylhä
Laboratory of Signal Processing
Tampere University of Technology
Tampere, Finland
firstname.lastname@tut.fi

***Abstract*—Applications such as radar performance prediction and automatic target recognition (ATR) require a compact description of the target and the ability to simulate target signatures fast. The complexity of the target model often slows the estimation of the radar cross section (RCS). We propose a target characterization method that uses two separate techniques to compress the information and to simplify the computations: employing a value for the maximum carrier frequency for the RCS and considering only nearly specular scattering. While the latter also affects the accuracy of the RCS, the compression maintains the main characteristics of the signature and hypothetically the validity for ATR. We present computation time and disk space comparisons showing the significant decrease in required resources. The effect of the compression level on the RCS values and distribution, and high range resolution profiles is visualized. A radar measurement is presented as a comparison to show the general validity of the simulation method.**

I. INTRODUCTION

Applications such as radar performance prediction and automatic target recognition (ATR) require a representation for targets that provide information on their radar signatures, e.g. the radar cross section (RCS). In ATR, there is typically a need for an extensive alterable target library, and for high-resolution radar, a wide bandwidth is also a requirement for each target [1]. This calls for a compact description of the target and the ability to simulate target signatures fast. In this paper, we introduce a method exploiting geometric optics (GO) for extracting the scattering properties of the target and consider compression techniques to obtain fast signature production.

GO estimates the RCS of a target efficiently using ray tracing or ray launching to calculate the illumination of the target. Since GO considers the transmission as a set of individual rays, certain kinds of phenomena—such as wave interference, diffraction, and polarization—are ignored. However, the GO computations can be performed very quickly compared with other methods such as physical optics (PO), especially in the case of multiple reflections. The inclusion of PO at the last point of reflection has been proposed in e.g. [2] to increase the accuracy of the GO result.

While the complexity of the simulation method increases the simulation time, so does the complexity of the target model. Targets are usually modeled as three-dimensional (3D) polygon meshes, most commonly consisting of triangles. We refer to these polygon meshes as "3D models". Regardless of the simulation method, 3D models are typical target characterizations in different software such as POFacets [3] and CAST [4]. In this paper, we use the term "target characterization" to refer to such a description of an object of interest that provides the necessary information—i.e. the scattering properties—for the RCS simulation.

To produce the most realistic result, the material and the shape of the 3D surface needs to correspond precisely to the real-life object it represents. However, the curved surfaces of many real-life targets are challenging and even impossible to reproduce with polygonal elements. A higher precision for the curved surface is attained by increasing the number of elements, but a higher polygon count does not guarantee higher precision. According to our experience, the achievable ATR capability is limited more by the general quality of the 3D model than by the minuscule details of the model or the chosen RCS simulation method. A perfect target characterization is not required for ATR; a few distinctive features of the target may be sufficient, but they can be absent from a low-quality 3D model. Altogether, it is challenging to estimate the quality of a 3D model in RCS simulation beforehand; the required accuracy is comparable with the radar wavelength and short wavelengths are unforgiving towards the 3D model. If the available 3D model is of a questionable quality, it is sensible to use a simpler simulation method than misspend the resources with a computationally extensive method while aspiring after the perfect response prediction.

Our solution for fast RCS computation is to compile an efficient target characterization using the result of the GO ray tracing. We exploit the concepts of antenna theory in the computation of the RCS to alleviate the shortcomings of GO. We have introduced these concepts in [5] and [6] in relation to radar response simulation and target recognition. In [7], we presented the ESPRESS (Electromagnetic Signature Production from Renders Exploiting Scatterer Sets) algorithm and extended the concepts for bistatic RCS. In this paper, we further develop these methods for fast monostatic RCS calculation and introduce a more efficient algorithm SPURT (Signature Production Using Ray Tracing). By employing different data compression levels in SPURT, our aim is to find a compromise between the fast calculation and sufficient RCS prediction accuracy for ATR.

The proposed algorithm shares the basic concepts of ESPRESS but it is implemented completely in MATLAB instead of exploiting a commercial ray tracing software. Monostatic SPURT (M-SPURT) is a fast version of the SPURT

algorithm, which increases the efficiency of the RCS simulation by compacting the target characterization further. With the assumption of monostatic operation, the information required for computing the RCS of one aspect angle for multiple frequencies reduces to the illuminated area of the target at different ranges. To further compress the information, we employ a value for the maximum carrier frequency f_{lim} the RCS is to be computed on, which influences the resolution of the ray tracing as well the quantization of the range values. As another compression technique, we consider discarding scatterers that reflect the ray less specularly. In this paper, we use the term "B-SPURT" (Bistatic SPURT) to discriminate the uncompressed version of SPURT from the M-SPURT; the "uncompressed" meaning that none of the scatterers are discarded and range values are not quantized, but the f_{lim} still affects the ray resolution.

II. M-SPURT

In SPURT, we use ray tracing to extract scatterer sets from the triangle mesh representation of the target. Each scatterer set contains information about the surface illuminated by radar at a particular aspect angle and is used as a target characterization. In B-SPURT, one scatterer set enables bistatic RCS simulation with various frequencies and receiver aspect angles; in M-SPURT, scatterer sets are more compact and each one enables monostatic RCS simulation with various frequencies. We define the aspect angle as an azimuth-elevation angle pair (az, el); e.g. (0°, 0°) is the observation at the front of the target. The azimuth angle is the angle about the vertical axis of the target ascending clockwise and the elevation angle is the angle from the horizontal plane of the target ascending upwards.

A. Variable Grid Density

In commercial ray tracing software, rays form an even-interval grid since the main purpose of such software is to produce visual images. We noticed that in ESPRESS, in the context of RCS estimation, this produces unwanted phenomena with certain surfaces, especially ones that are nearly parallel to the direction of the observation, when the rays hit the surface too sparsely. We propose mending this by creating a variably dense grid of rays.

To create a grid of rays with a variable density, we cover the visible triangles of the 3D model of the target with preliminary ray positions. From the preliminary positions, only those that are visible to the radar are selected as computation rays and those that are shadowed by the target itself are discarded; this is important especially with large triangles. The preliminary ray grid density is dimensioned according to the f_{lim} in order to create a frequency-independent target characterization, which is achieved as long as the spacing between the rays is at most half the operating wavelength λ [6]. This derives from the fact that the scatterers are analogous with a uniform linear array of antenna elements, and the maximum acceptable spacing between two such elements is $\lambda/2$ with the maximum desired look angle of 90° to avoid severe grating lobes [8].

The variably dense ray grid is used as an input to a simple ray tracing algorithm. Each ray is traced from the radar transmitter to the target and bounced on the surface of the target until either it has finally bounced away from the target or a predefined maximum number of bounces has been reached. This technique is actually called ray launching, but considering monostatic radar, ray launching and ray tracing are equivalent. The commercial ray tracing software used by ESPRESS was unable to track the overall distance of the multi-bounce rays, which induced some error; in SPURT, this was trivial to fix.

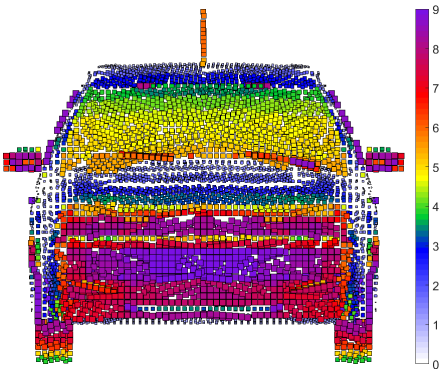

Fig. 1. The variably dense ray grid of Volkwagen Golf (see Section III for more information) at the aspect angle (0°, 0°) using f_{lim} = 5 GHz (λ_{lim} = 6 cm). Each square represents a single ray. The size and the color of the square correspond to the ray contribution area; the values are in cm^2. The areas are represented as squares, since the scatterers are treated as square plates later in the simulation phase, but their actual shapes vary.

Each computed ray has a contribution area depending on the ray grid density. The maximum ray grid interval is defined by λ_{lim}, the radar wavelength corresponding to f_{lim}. The corresponding ray contribution area is $(\lambda_{\mathrm{lim}}/2)^2$ for a surface perpendicular to the ray direction; the more slanted the surface, the smaller the contribution area due to the projection. An example of a variably dense ray grid and ray contribution areas is presented in Fig. 1.

Each ray transforms to a single scatterer and a scatterer set corresponds to a single radar transmitter aspect. Typically, it is adequate to employ a resolution of one degree in both the azimuth and elevation directions—resulting in a grid of 181×360, or 65160, aspect angles. A denser sampling of the aspect angles is required e.g. in synthetic aperture radar (SAR) simulation.

B. Data Compression

Both the ray tracing time and the disk space required to save the scatterer sets are dependent on the physical dimensions of the target and f_{lim}—a larger target and a higher f_{lim} needing a larger set and more time. Although the ray tracing is the most time consuming part of the process, it does not have to operate in real time; once the scatterer sets are constructed, they can be used in real time applications, which sets higher requirements on the RCS simulation.

While the bistatic RCS computation requires several different variables for each scatterer, a monostatic scatterer is fundamentally reduced to the distance traveled by the ray and the ray contribution area. Scatterers can be further compressed by adding the areas at the same distance together. In reality, few scatterers are at the same exact distance from the radar. The quantization of the distance information with a small factor Δ_{d} aids the compression further; however, the quantization must not interfere with f_{lim}; e.g. $\Delta_{\mathrm{d}} \leq \lambda_{\mathrm{lim}}/16$.

The summation of the areas of different scatterers imposes the assumption that the scatterers have uniform reflectivity. In reality, the reflectivity of a single scatterer shaped as a square plate has a form of a sinc function depending on the angle between the scattered ray and the receiver direction [8]. Thus, assuming uniform reflectivity induces some error. The effect of the sinc function is minimal with low frequencies and ascends with the frequency. However, even using a frequency of 15 GHz, the maximum error is about 10 % when likely targets are concerned. Henceforth, the group of scatterers at the same distance is considered as a single M-SPURT scatterer at a unique distance.

Another way to compress the data, albeit lossily, is to discard scatterers that reflect the ray less specularly. We have constructed a comparison of nine different angle limits for the retroreflectivity or the reflection specularity: 180° (no limit), 90°, 60°, 30°, 25°, 20°, 15°, 10°, and 5°. We call these retroreflectivity limits—henceforth denoted with Φ—and they define the maximum angle between the incident ray and the reflected ray (illustrated in Fig. 2); the term "retroreflectivity angle" is used for this angle. We hypothesize that this kind of compression preserves the main characteristics of the RCS although the precise values are subject to change.

In the case of a single-bounce contact and monostatic radar, only rays with an angle of incidence less than or equal to Φ/2 are taken into account, since the angle of incidence is half the retroreflectivity angle in a specular reflection. With a multi-bounce contact, the retroreflectivity angle is the angle between the original incident ray and the final direction of the reflected ray. A virtual single-bounce normal is defined as the bisector of the retroreflectivity angle. Regardless of the Φ, the surface of the final contact shadows the other side, and thus the visibility of each scatterer is always at most a hemisphere.

C. Radar Response Simulation

The RCS simulation in M-SPURT is essentially the same as in [7], but slightly simpler and noticeably faster due to the simplified nature of the monostatic case. The perpendicular RCS σ_d, i.e. the power of the specular reflection, of a square plate depends on the area A_d of the plate:

$$\sigma_d = 4\pi \frac{A_d^2}{\lambda^2}, \tag{1}$$

where λ is the operating wavelength of the radar [9]. As mentioned in Section II.A, we use uniform reflectivity for each M-SPURT scatterer to achieve a higher data compression level, and A_d corresponds to the ray contribution area of the M-SPURT scatterer at a unique two-way distance d (the sum of the distance to the transmitter and the distance to the receiver). The phase of the scatterer at a distance d is

$$\varphi_d = \frac{-2\pi d}{\lambda}. \tag{2}$$

At a particular aspect angle, the RCS of a target is a coherent sum of the RCS at different distances:

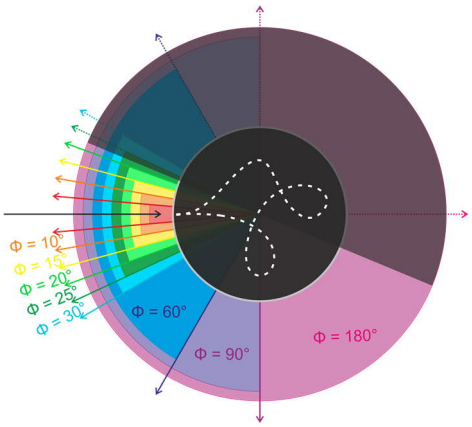

Fig. 2. Nine retroreflectivity limits used in our experiments. The traced ray (the black arrow) approaches an undefined target (the black circle) from the left. The target can be considered as a "black box" since we are not interested in the path of the ray (the white dashed line) but the length and the final direction of it. After a number of bounces, the ray exits the target and the surface of the final contact shadows the other side of the surface (an arbitrary choice shown as a gray shadow). The resulting scatterer is visible only to the receivers on the light side; thus in the monostatic case, the scatterer is visible to the radar if the black arrow is on the light side (as it is in this case). The figure also shows nine pairs of rays (one at each Φ), which delimit the sectors representing the angular span of the exiting rays that are contained in the corresponding scatterer set; e.g. if the ray exits the target between the two red arrows representing Φ = 5° (as the white dashed line does), the scatterer is present in all test cases. Since the presented white dashed line path is arbitrary, the ray can exit at any direction; in a case of a single-bounce contact, the ray would exit at the sector of Φ = 180°.

$$\sigma = \left(\sum_d \sqrt{\sigma_d}\, e^{-i\varphi_d} \right)^2. \tag{3}$$

III. Results

In this section, we present RCS and high range resolution (HRR) profiles simulated with M-SPURT using multiple values for Φ, as well as examples of the scatterer sets used as the target characterization. The RCS is also considered as a distribution and compared with a radar measurement using two distance measures. We also compare computation time and file size.

The main objective of these experiments is to show the effect of the chosen Φ on the compression level and the simulated response. Instead of aspiring after a perfect target characterization, our aim is to find the highest possible compression level without hindering a real-life ATR system. Thus, a general validation of the SPURT method is done through a comparison with a radar measurement—which is the baseline for the ATR—instead of other RCS simulation methods. When applicable, the B-SPURT result is also presented for comparison. B-SPURT produces the best possible result that can be achieved using the SPURT method and the 3D model in question and thus, the feasibility of the proposed compression method is verified by comparison with the B-SPURT result rather than the measurement.

The target we consider in these results is Volkswagen Golf; the 3D model of which has been acquired from the Trimble 3D Warehouse. Unless otherwise stated, f_{lim} = 15 GHz and a transmitter frequency of 3 GHz are used in the presented

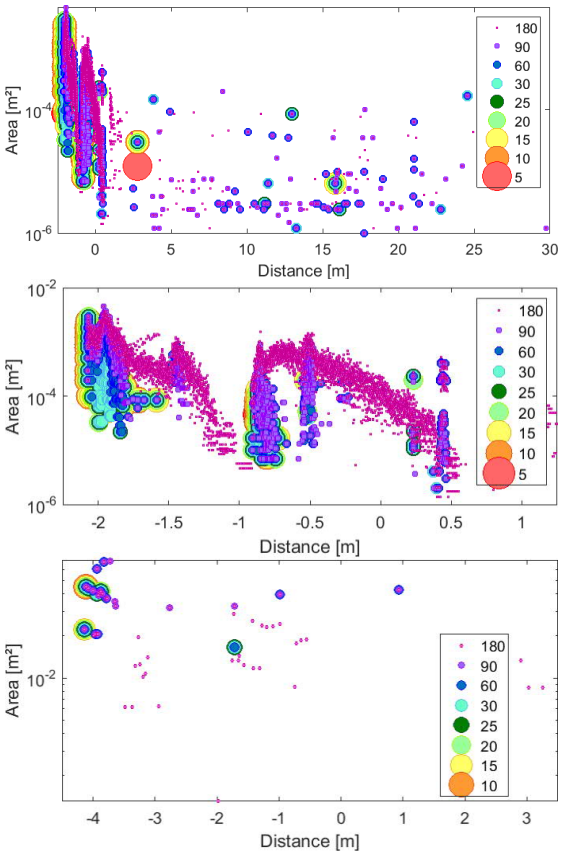

Fig. 3. The scatterer sets of Volkswagen Golf with various values of Φ at aspect angle (0°, 0°). Each scatterer, represented by a colored circle, consists of a unique two-way distance from the target center point and the corresponding area. Note that the y axis has a logarithmic scale. On the top: f_{lim} = 15 GHz; in the middle: a detail of f_{lim} = 15 GHz at small distances, and on the bottom: f_{lim} = 1 GHz.

simulations. The measurement setup and the measured vehicle used in this paper have been described in more detail in [6]. The 3D model and the actual measured vehicle have some differences in the shape as well as the material information in the simulation; the simulation has been performed considering the target as a perfect electric conductor and the shape differs e.g. in the hubcaps of the vehicle. Thus, the 3D model used would not offer the best possible results if the performance of the ATR system was under evaluation, but does not intervene in the comparison of the effects of Φ.

A. The Scatterer Sets

The M-SPURT scatterer set consists of a unique two-way distance from the target center point and the corresponding area. The number of scatterers of Volkswagen Golf at the radar aspect (0°, 0°) using nine different values of Φ and B-SPURT, and two values for f_{lim} are presented in Table I. The chosen aspect angle affects the number of scatterers and these sets are among the smallest ones of Volkswagen Golf. The M-SPURT scatterer sets

TABLE I. SCATTERER NUMBERS OF VOLKSWAGEN GOLF AT (0, 0)°

	B-SPURT	***180°***	***90°***	***60°***	***30°***	***25°***	***20°***	***15°***	***10°***	***5°***
15 GHz	62120	5388	1445	1050	487	383	290	201	104	5
1 GHz	95	52	22	16	6	6	3	2	1	0

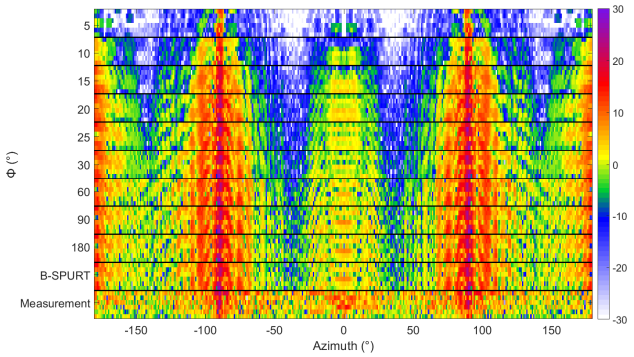

Fig. 4. The RCS of Volkswagen Golf using nine different values of Φ and the corresponding uncompressed B-SPURT and the measurement; from top to bottom Φ = 5°, 10°, 15°, 20°, 25°, 30°, 60°, 90°, 180°, and B-SPURT and the measurement. Each RCS matrix has 6 × 360 elements; the axis values ranging from 10° to 0° in elevation from top to bottom and from −180° to 179° in azimuth from left to right. The RCS values, presented with different colors, are in dB(m²).

of Volkswagen Golf with the nine different values of Φ at (0°, 0°) using f_{lim} = 15 GHz and Δ_d = 1.0 mm, and f_{lim} = 1 GHz and Δ_d = 1.0 cm are shown in Fig. 3. The figure shows the refinement in the structure of the scatterer set as the Φ increases—as the Φ decreases, only the most dominant scatterers remain. The distances beyond the length of the car are due to the multi-bounce rays.

B. The RCS Comparison

Fig. 4 shows the simulated RCS of Volkswage Golf using nine different values of Φ, B-SPURT, and the measurement for a 6×360 aspect angle grid. The gradual enhancement of the result is evident as the Φ increases; as Φ decreases and more scatterers are discarded, the simulated response becomes more simplistic. While there are local differences between the measurement and the simulation, they are still about the same magnitude.

The method proposed in [10] is used to calculate RCS distributions for each Φ, B-SPURT, and the radar measurement. As an example, the distributions of Φ = 180° and the measurement are shown in Fig. 5, as well as medians of the distributions; some values of Φ are omitted for clarification. The medians of B-SPURT and Φ = 180° match almost perfectly and Φ = 60° differs only slightly from them. All these three are clearly similar to the measurement, which has less variation across the azimuth angles than the simulations do. While the shape of the RCS distribution is similar even with the smallest values of Φ, their median is notably lower than the measurement.

The similarity of the RCS distributions is examined with the Bhattacharyya distance (BD) [11] and earth mover's distance (EMD) [12], which both are distance measures to quantify the similarity between two probability distributions. Both distance measures for each azimuth angle are calculated between all possible combinations and they are shown in Fig. 6. In most cases, the front, the back, and the sides of the target are more similar than the diagonal directions. This is not surprising, since large areas of the model surface face at these directions, and thus, they are present in all scatterer sets. While all combinations are presented, the comparison with the measurement gives a rough estimate for the validity of the characterization, and especially the comparison with the B-SPURT shows the effect

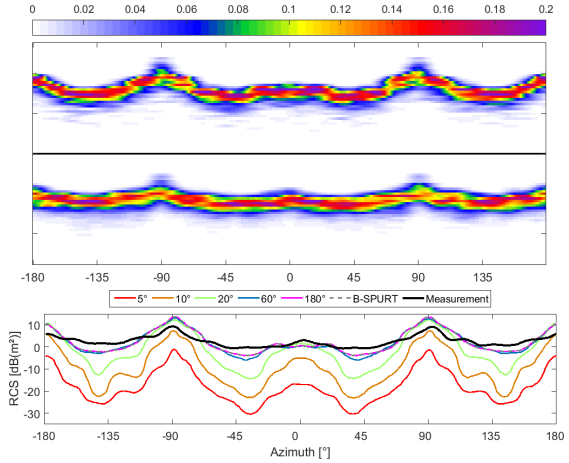

Fig. 5. Examples of RCS distributions and their medians at elevation angle of 0°. The azimuth ranges from −180° to 179° horizontally. On the top and in the middle, each column in the image represents a normalized RCS histogram at the corresponding azimuth angle. On the top: the RCS distribution of Φ = 180°; in the middle: the RCS distribution of the measurement; on the bottom: the medians of the distributions calculated with several values of Φ.

of the data compression. In this case, the Φs of 180° and 60° produce quite similar results as the B-SPURT according to the distance measures. Most importantly, the figure shows the relative impairment of the simulation quality when the Φ decreases—the actual values being less interesting. Median EMD and BD values are presented in Table II; some values of Φ are omitted. EMD is expressed as a percentage; 0 % represents identical distributions and 100 % represents comparing a histogram with all the weight in the first bin [1, 0, 0, …] with a one with all the weight in the last bin [0, 0, …, 1]. For example, the maximum value of EMD in Fig. 6—14.8—equals 32.9 % (with 46 bins).

The simulated and measured HRR profiles of the Volkswagen Golf are presented in Fig. 7. Such a profile is obtained by integrating over a wide frequency band. We have used a center frequency of 9 GHz and a bandwidth of 2 GHz resulting in a range resolution of 7.5 cm. Again, the main characteristics are similar in each case, which validates the phase angle information and the compression applied to it.

C. The Hard Disk Consumption

In this subsection, we compare the hard disk consumption of the M-SPURT scatterer sets with the corresponding B-SPURT scatterer sets. Table III shows the disk space requirements for the Volkswagen Golf using f_{lim} = 1 GHz and f_{lim} = 15 GHz. Between B-SPURT and M-SPURT, the required disk space decreases at least by 98 % for the Volkswagen Golf with the

TABLE II. THE MEDIAN PROBABILITY DISTRIBUTION DISTANCES

	B-SPURT	***180°***	***60°***	***30°***	***20°***	***15°***	***10°***	***5°***
BD to Measurement	0.056	0.057	0.066	0.096	0.17	0.29	0.63	1.3
BD to B-SPURT	0	0.0017	0.015	0.046	0.11	0.22	0.53	1.2
EMD (%) to Measurement	3.2	3.2	3.5	4.1	5.5	9.0	15	25
EMD (%) to B-SPURT	0	0.051	0.69	1.7	4.4	7.4	14	23

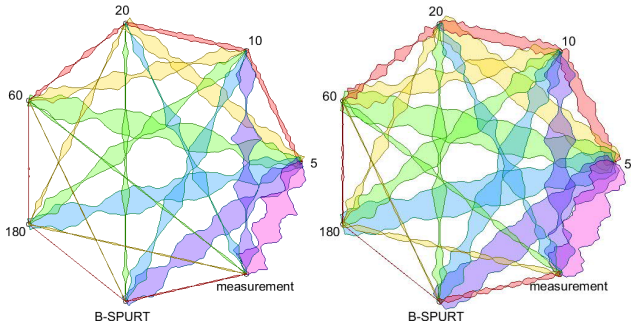

Fig. 6. The distance measures of the RCS distributions calculated with different values of Φ, B-SPURT and the measurement. On the left: the BD; and on the right: the EMD. Each RCS distribution is compared with all the other distributions; the lines with a variable width represent the distance between the two cases at the endpoints of the line. The azimuth angle increases along the line—the back of the target is at the endpoints of the line and the front of the target is in the middle. The true values of the BD range from 0 to 2.75 and the EMD from 0 to 14.8.

maximum frequency of 15 GHz: the B-SPURT scatterer sets have an average size of 3300 kB per aspect angle and the M-SPURT sets with Φ = 180° have an average size of 53 kB per aspect angle. With Φ = 5°, the scatterer sets have an average size as small as 0.42 kB—resulting in a decrease of almost 99.99 % in the required disk space (shown as 0.012 % of B-SPURT in the table). Thus, using the predefined resolution of 65160 aspect angles per target, such a target would need disk space from approximately 27 MB (Φ = 5°) to 3.3 GB (Φ = 180°) compared with the original 210 GB of the uncompressed B-SPURT.

D. Computation Time

The computation times in this subsection were obtained with a standard desktop computer. The hardware used affects the computation time, but more important than the actual values is the relative change in them. Using f_{lim} = 15 GHz, the ray tracing time for Volkswagen Golf is about 170 minutes per aspect angle; the choice of B-SPURT or M-SPURT does not affect it. Using B-SPURT, the monostatic RCS simulation takes about 0.43 s per aspect angle. With M-SPURT, the calculation time for a single aspect angle is about 0.25 s, which is only slightly better than B-SPURT. However, the effectiveness emerges when several aspect angles are calculated simultaneously. Calculating a 21×360 element grid of aspect angles takes about 18 minutes with B-SPURT. With M-SPURT, the simulation takes about 8.4 seconds when Φ = 180° and as little as 0.49 seconds when Φ = 5°. Thus, M-SPURT decreases the simulation time by over 99 %

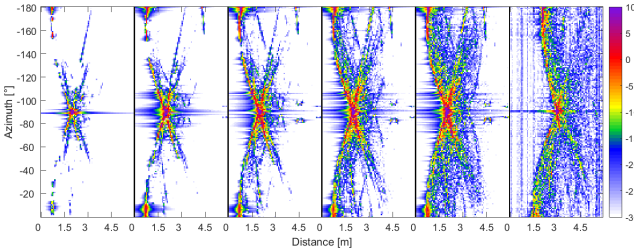

Fig. 7. The HRR profiles of a Volkswagen Golf in the elevation angle of 0° using different values of Φ and a radar measurement; from left to right: Φ = 5°, 10°, 20°, 60°, 180°, and a radar measurement. In each case, only the left side of the target is presented. From the top to the bottom of the image, the target rotates in azimuth. The range from the radar increases from left to right; each case ranging 6 meters in total. The RCS values, presented with different colors, are in dB(m²).

TABLE III. REQUIRED DISK SPACE FOR VOLKSWAGEN GOLF

	Average file size / aspect (kB)		*Whole target (MB)*		*% of B-SPURT*	
f_{lim}	*1 GHz*	*15 GHz*	*1 GHz*	*15 GHz*	*1 GHz*	*15 GHz*
B-SPURT	15	3300	990	210000	100	100
180°	1.2	53	77	3400	7.8	1.6
90°	0.61	28	39	1800	3.9	0.83
60°	0.34	17	21	1100	2.2	0.52
30°	0.12	6.8	7.4	430	0.75	0.20
25°	0.09	5.3	5.7	340	0.58	0.16
20°	0.066	3.8	4.2	240	0.43	0.11
15°	0.044	2.4	2.8	150	0.28	0.071
10°	0.025	1.3	1.6	80	0.16	0.037
5°	0.012	0.42	0.74	27	0.075	0.012

making it reasonably fast even for real-time applications. This comparison of B-SPURT and M-SPURT reveals the value of the proposed simplifying approximations concerning the computation time. The computation times of Volkswagen Golf are presented in Table IV; the values are in seconds for a 21×360 aspect angle grid. With f_{lim} = 1 GHz, the ray tracing time is about 36 seconds per aspect angle for Volkswagen Golf. The RCS computation times vary from 0.27 s to 0.44 s in M-SPURT compared with the 4.3 s of B-SPURT for the 21×360 aspect angle grid.

IV. DISCUSSION AND CONCLUSIONS

In this paper, we introduced the M-SPURT algorithm for fast monostatic RCS simulation. The effectiveness is achieved by compiling a target characterization in a form of a scatterer set that has been compressed using various techniques: employing a value for the maximum carrier frequency for the RCS and considering only surfaces nearly perpendicular towards the radar. The former includes quantizing the range information by a small value and combining scatterers at the same range, and the latter is influenced by the retroreflectivity limit, Φ.

The presented results show that the proposed method produces good results; the calculation is fast, the hard disk consumption is manageable, and the produced RCS corresponds to the measurement well. As can be seen in Fig. 4 by comparing the result of B-SPURT and M-SPURT with Φ = 180°, the compression achieved by combining scatterers with the same range and quantizing the range information does not cause significant error in the RCS. In addition to these two compression techniques, the slight differences between these results are due to the omission of the sinc function in M-SPURT.

We presented results for nine different values of Φ, from which only one would be chosen for practical use. The decision of the proper value is a compromise between the accuracy and the computation speed. Although the differences in the calculated RCS using various values of Φ are visually evident, in applications, where close to real-time operation is preferred, the choice of a lower value may be justified. In ATR for instance, few strong dominant features might just be enough to distinguish between different types of targets. This requires further investigation.

TABLE IV. THE RCS COMPUTATION TIME OF VOLKSWAGEN GOLF

	B-SPURT	*180°*	*90°*	*60°*	*30°*	*25°*	*20°*	*15°*	*10°*	*5°*
15 GHz	1100	8.4	4.4	2.8	1.3	1.0	0.87	0.60	0.50	0.49
1 GHz	4.3	0.44	0.36	0.33	0.30	0.30	0.29	0.29	0.28	0.27

The most important result in this paper is the proven feasibility of the proposed compression method. In general, SPURT seems promising for model-based ATR, offering a reasonable computation time for wide bandwidth simulations. The single-target analysis presented in this paper should not be considered as an indication of the actual performance regarding ATR; our future plans include conducting a feasibility study for M-SPURT concerning the ATR of several practical targets.

ACKNOWLEDGMENTS

This research was conducted with funding from the Finnish Defence Forces Research Program 2017 and the Finnish Scientific Advisory Board for Defence. The authors would like to thank the Finnish Defence Forces and Patria Aviation for support and successful co-operation.

REFERENCES

[1] K. El-Darymli, E. W. Gill, P. Mcguire, D. Power, and C. Moloney, "Automatic target recognition in synthetic aperture radar imagery: a state-of-the-art review," IEEE Access, vol. 4, pp. 6014–6058, Sep. 2016.

[2] H. Ling, R. C. Chou, S. W. Lee, "Shooting and bouncing rays: calculating the RCS of an arbitrarily shaped cavity", IEEE Transactions on Antennas and Propagation, vol. 37, no. 2, pp. 194–205, Feb. 1989.

[3] F. Chatzigeorgiadis, D. C. Jenn, "A MATLAB physical-optics RCS prediction code", IEEE Antennas and Propagation Magazine 46.4 (2004): 137–139.

[4] Tool for Radar Cross Section Calculation [Online]. Available: http://virtual.vtt.fi/virtual/proj2/cast/

[5] H. Perälä, M. Väilä, J. Jylhä, I. Venäläinen, A. Visa, "Converting a 3D surface into a set of directional scatterers for high-resolution radar response simulation", Proc. SPIE 8134, Optics and Photonics for Information Processing V, 81340H (Sept. 21, 2011).

[6] H. Perälä, M. Väilä, J. Jylhä, J. Kylmälä, V.-J. Salminen, A. Visa, "On efficient characterization of radar targets with scatterer sets for target recognition using commercial ray tracing software", IEEE Radar Conference, 2014.

[7] H. Perälä, M. Väilä, J. Jylhä, A. Visa, "ESPRESS—On efficient bistatic characterization of radar targets", IEEE Radar Conference, 2015.

[8] G. W. Stimson, Introduction to Airborne Radar (2nd Edition), SciTech Publishing, Inc., Raleigh, North Carolina, USA, 1998.

[9] E. F. Knott, J. F. Shaeffer, M. T. Tuley, Radar Cross Section (2nd Edition), SciTech Publishing, Inc., Raleigh, North Carolina, USA, 2004.

[10] M. Väilä, J. Jylhä, T. Sailaranta, H. Perälä, V. Väisänen, A. Visa, "Incorporating a stochastic model of the target orientation into a momentary RCS distribution", IEEE Radar Conference, 2015.

[11] T. Kailath, "The divergence and Bhattacharyya distance measures in signal selection", IEEE Transactions on Communication Technology, vol. 15, no. 1, pp. 52–60, February 1967.

[12] Y. Rubner, C. Tomasi, and L. J. Guibas, "A metric for distributions with applications to image database," Sixth International Conference on Computer Vision, p. 59-66, 1998.